Simulation of Fourth-Order Laterally-Coupled Gratings

R. Millett, A. Benhsaien, K. Hinzer, T. Hall and H. Schriemer*
Centre for Research in Photonics, University of Ottawa
*Corresponding author: 800 King Edward Ave., Ottawa, ON, K1N 6N5, hschriem@site.uottawa.ca

Abstract: We have developed a technique using COMSOL Multiphysics to calculate the effective coupling coefficient, κ_{eff}, of higher order laterally-coupled gratings. We apply this model to the case of a fourth-order grating and determine that there are local maxima in $|\kappa_{eff}|$ at duty cycles of 0.58 and 0.88, that there are periodic variations in κ_{eff} with grating height, and $|\kappa_{eff}|$ generally grows as the grating ridge width ratio W_N/W_W decreases.

Keywords: modified coupled-mode analysis, distributed feedback lasers, higher order gratings.

1. Introduction

Distributed feedback lasers improve the performance of standard Fabry-Perot laser designs by including a wavelength-selective grating that provides superior output, spectral purity and temperature stability. Laterally-coupled distributed feedback (LC-DFB) lasers, such as our design shown in Figure 1, have a grating that has been patterned out of the waveguide ridge [1,2]. This allows for simplified fabrication and monolithic integration with a variety of other photonic devices. The fabrication of LC-DFB lasers can be further simplified with the use of higher order gratings, i.e. using integer multiples of the first-order Bragg grating period. As an example, our application, a 1310 nm laser, uses a fourth-order grating with a period of 800 nm, making it easier to fabricate using standard lithographic techniques compared to a first-order grating with a period of 200 nm.

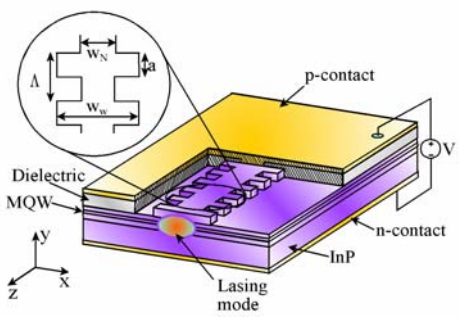

Figure 1. Cutaway view of laterally-coupled distributed feedback laser.

2. Modified Coupled-Mode Analysis

2.1. Theory

The modified coupled-mode equations, first derived by Streifer *et al.*, are [3]:

$$\begin{aligned} \frac{dA}{dz} + \left(-\alpha - j\delta - j\zeta_1\right)A &= \left(\kappa_p^* + \zeta_2\right) \\ -\frac{dB}{dz} + \left(-\alpha - j\delta - j\zeta_3\right)B &= \left(\kappa_p + \zeta_4\right) \end{aligned} \tag{1}$$

where α is the modal gain/loss, δ is the Bragg frequency detuning, κ_p is the coupling coefficient, A and B are the longitudinal mode field amplitudes, and $\zeta_{1,\ldots,4}$ are the Streifer correction terms.

The calculation of the modified coupled-mode coefficients, κ_p and $\zeta_{1,\ldots,4}$, for fourth-order gratings is the focus of this paper. The first step is to find the quasi-TE mode solution of the Helmholtz wave equation:

$$\begin{aligned} &\frac{\partial^2 \varepsilon_0(x,y)}{\partial x^2} + \frac{\partial^2 \varepsilon_0(x,y)}{\partial y^2} \\ &+\left[k_0^2 n_0^2(x,y) - \beta^2\right]\varepsilon_0(x,y) = 0 \end{aligned} \tag{2}$$

where ε_0 is the modal field, and β is the propagation constant. The quasi-TE solution of Equation (2) is used to calculate κ_p, where p=-N, and N is the grating order:

$$\kappa_{-4} = \frac{k_0^2}{2\beta P}\iint_G A_{-4}(x,y)\varepsilon_0^2(x,y)dxdy \tag{3}$$

where k_0 is the free-space wavenumber, P is the power contained in the optical mode, G is the grating region, and A_{-4} is the Fourier coefficient

of the grating. For the fourth-order rectangular gratings studied here, the Fourier coefficients are [4]:

$$A_{-4} = A_4 = -\frac{\left(n_2^2 - n_1^2\right)}{4\pi}\sin\left(4\pi\gamma\right) \qquad (4)$$

The duty cycle is defined as $\gamma = a/\Lambda$, where a is the wide ridge length, and Λ is the grating period, referring to Figure 1, and $n_{1,2}$ are the low and high refractive indices, respectively, along the length of the grating. The larger index, n_2, is the average index of the semiconductor grating region layers, and the smaller index, n_1=1.445, is the index of the SiO_2 dielectric. The Fourier coefficients vanish outside of the periodic grating, resulting in the integration of Equation (3) being only over the grating region.

To calculate the $\zeta_{1,\ldots,4}$ terms, partial waves of order m, for both forward and backward waves (i=0,p), $\varepsilon_m^{(i)}$, must be solved. These partial waves can be obtained from solutions to the modified wave equation [5]:

$$\frac{\partial^2 \varepsilon_m^{(i)}(x,y)}{\partial x^2} + \frac{\partial^2 \varepsilon_m^{(i)}(x,y)}{\partial y^2} + \left[k_0^2 n_0^2 - \beta_m^2\right]\varepsilon_m^{(i)}(x,y) = -k_0^2 A_{m-i}(x,y)\varepsilon_0(x,y) \qquad m \neq i, i = 0, p \qquad (5)$$

where $\beta_m = \beta_0 + 2\pi m/\Lambda$ is the propagation constant of the partial wave of order m, and β_0 is the propagation constant for the Bragg grating condition. The $\zeta_{1,\ldots,4}$ terms are obtained from the partial wave solutions by

$$\begin{aligned}
\zeta_1 &= \sum_{\substack{q=-\infty \\ q\neq 0,4}}^{\infty} \eta_{q,-q}^{(0)} \\
\zeta_2 &= \sum_{\substack{q=-\infty \\ q\neq 0,4}}^{\infty} \eta_{q,-q}^{(-4)} \\
\zeta_3 &= \sum_{\substack{q=-\infty \\ q\neq 0,-4}}^{\infty} \eta_{q,-4-q}^{(-4)} \\
\zeta_4 &= \sum_{\substack{q=-\infty \\ q\neq 0,-4}}^{\infty} \eta_{q,-4-q}^{(0)}
\end{aligned} \qquad (6)$$

where

$$\eta_{r,s}^{(i)} = \frac{k_0^2}{2\beta P}\iint_G A_r(x,y)\varepsilon_0(x,y)\varepsilon_s^{(i)}(x,y)dxdy \qquad (7)$$

The total coupling of the higher order grating, including contributions from the $\zeta_{1,\ldots,4}$ terms, can be expressed by an effective coupling coefficient, κ_{eff} [6]:

$$\kappa_{eff} = \sqrt{\left(\kappa_{-4}^* + \zeta_2\right)\left(\kappa_{-4} + \zeta_4\right)} \qquad (8)$$

The real part of κ_{eff} will give the amount of index coupling, while the imaginary part expresses the amount of gain/loss coupling of the grating.

2.2. Numerical Solution

The numerical solution begins with the quasi-TE mode solution of Equation (2). The particular structure of used here has been previously described in [7]. The solution is found using the Perpendicular Hybrid-Mode Waves application mode of the COMSOL RF Module; this calculates the mode field and the effective index of the fundamental TE mode. The adaptive mesh feature is used to refine the initial mesh. The computational domain is 8 μm in height and 8 μm in width. Perfect electric conductors are used at the boundaries; these are sufficiently removed from the guided mode field to have a negligible impact on the solution.

The solution of this problem results in a range of modes. To obtain the quasi-TE mode, $\varepsilon_0(x,y)$, an overlap of the electrical field in the x-direction, E_x, with a Gaussian waveform is performed. The quasi-TE mode is the one with the largest overlap. From this solution, the propagation constant is determined, and Equation (3) can be evaluated using the subdomain integration feature with only those subdomains that comprise the grating region.

The modal field of $\varepsilon_0(x,y)$ is then saved to a data file to be used in the solution of Equation (5). The solution of Equation (5) is obtained using the Helmholtz wave equation module of COMSOL. The source term uses the modal field, obtained from the data file. The partial wave terms use a computational area 15 μm high and 14 μm wide. Since this area is larger than

the calculation window of the modal field, $\varepsilon_0(x,y)$ is assumed to be zero outside the original computational window size. This has been numerically verified to have a negligible impact on the solutions, since the source term only appears in the grating regions, far from the computational window boundaries of both solutions. The partial waves of lower orders are often radiative. To generate the correct modal fields without resorting to an excessively large computational window, absorbing boundary layers were used. In these layers, the real part of the refractive index was kept the same as the adjoining subdomain, while the imaginary part

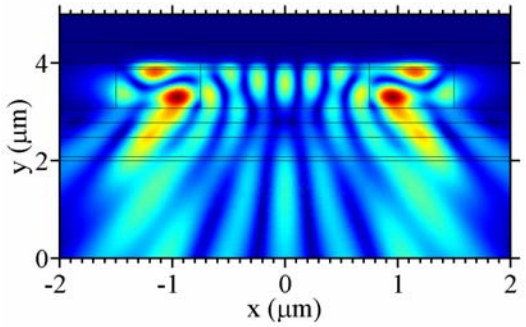

Figure 2. Detail of 1st order radiating partial wave of a laterally-coupled distributed feedback laser

increased quadratically towards the outer boundary. An example of an m=-1 radiating partial wave for a laterally-coupled grating is shown in Figure 2. The field is largest in the grating regions on either side of the ridge, where the source terms are nonzero. Outside these regions, resonances occur due to reflections from layers of different semiconductor materials or from the metal layers above the ridge. The metal layers are sufficiently reflective to prevent any light from escaping above the ridge.

The expressions for the $\zeta_{1,\ldots,4}$ terms include infinite summations that must be truncated for numerical evaluation. The number of partial wave orders that must be calculated was examined by Streifer, who found that partial wave orders from $-8 \le q \le 5$ was sufficient [4], while Zhong *et al.* used orders from $-12 \le q \le 10$ [8]. For our results, it was found that the coupling coefficient values converged to within 0.1% of a solution using partial wave orders from $-25 \le q \le 25$ when using only partial wave orders from $-9 \le q \le 9$. These are the partial wave orders that are used in the subsequent simulations. This range of partial wave orders is used in all subsequent calculations. The results of our method had agreed within 5% of the calculations by Zhong *et al.* [8].

3. Results

3.1. Duty cycle

The duty cycle, γ, of the grating is the ratio of the wide part of the ridge, a, to the total grating period, Λ, or $\gamma = a/\Lambda$. In rectangular gratings, the duty cycle will determine the Fourier coefficient of the grating, and thus have a direct effect on the coupling coefficient. While the Fourier coefficient is symmetrical around γ=0.5 for these gratings, κ_{eff} is larger for higher duty cycles, as shown in Figure 3. This is due to a higher average refractive index in the grating regions when the duty cycle is higher, resulting in a higher optical grating confinement and hence greater coupling.

There are four peaks in the $|\kappa_{eff}|$ *vs.* γ characteristic, the two largest are at γ=0.58 and 0.88 where $|\kappa_{eff}|$ = 29.8 and 85.0 cm^{-1}, respectively. The zero crossings of the phase characteristic are points where two degenerate longitudinal modes will both be supported, and should be avoided. They occur at duty cycles of 0.35 and 0.65.

3.2. Grating Height

We next examine the effective coupling coefficient for grating heights larger than 0.4 μm. At smaller grating heights, the optical mode will

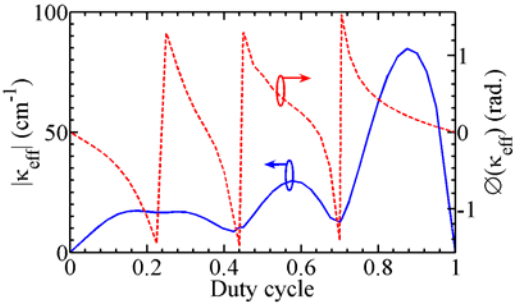

Figure 3. Magnitude, $|\kappa_{eff}|$, and phase, $\phi(\kappa_{eff})$, of the effective coupling coefficient *vs.* duty cycle for a fourth-order grating with W_N/W_W = 1.5/3 (μm).

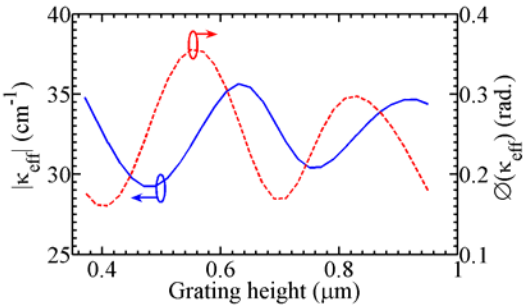

Figure 4. Effective coupling coefficient *vs.* grating height for a fourth-order grating with W_N/W_W = 1.5/3 (μm) and a duty cycle of 0.6.

be close enough to the metal contacts above the ridge to significantly increase the optical loss. The real and imaginary parts of κ_{eff} demonstrate damped oscillations as the height increases. The phase of these damped oscillations does not coincide for the real and imaginary parts. The real and imaginary part have a periodicity of ~0.3 μm, with a variation of ~5 cm^{-1} in $|\kappa_{eff}|$ and 0.15 radians in $\phi(\kappa_{eff})$. The ζ_2 terms are responsible for the oscillatory behaviour of the effective coupling coefficient.

At particular grating heights, the resonances that can be observed in Figure 2 become stronger or weaker, resulting in oscillations in the real and imaginary portions of κ_{eff}, as shown in Figure 4. These periodic variations will be larger when the contribution of ζ_2 to κ_{eff}, compared to κ_p, is relatively larger. The first peak in $|\kappa_{eff}|$ occurs at a grating height of 0.64 μm, this represents a stable point of fabrication for a strong laterally-coupled grating.

3.3. Grating Width

The effect of ridge width on the coupling coefficient has previously been studied by Choi [2], who found that the coupling coefficient decreases as W_N increases for a fixed W_W. We obtain a similar result for fourth-order gratings, shown in Figure 5(a). In addition, we observe subtle resonances in the $|\kappa_{eff}|$ *vs.* $W_{N,W}$ characteristic, and significant resonances in the $\phi(\kappa_{eff})$ *vs.* $W_{N,W}$ characteristic. The value of W_N should be made as small as possible to maximize $|\kappa_{eff}|$. This will be restricted by the minimum size required to place a metal contact on top of the ridge, typically around 1.5 μm.

We fix the W_N value to be 1.5 μm in Figure 5(b) and increase W_W from 1.5 to 4 μm. Similar resonances are observed as with the W_N characteristic, but the changes in $\phi(\kappa_{eff})$ tend to become more damped as $|\kappa_{eff}|$ saturates at ~30 cm^{-1} at wide ridge widths of 2.75 μm and above. The value of κ_{eff} is more sensitive to W_N than to W_W since the value of the dimensions of the ridge nearest the waveguide mode will tend to dominate. This is due to the fact that $\varepsilon_0(x, y)$ will drop off exponentially in the grating region away from the waveguide ridge, weighting the integrations of Equations (3) and (7) towards the waveguide ridge. From Figure 5, we can say that using W_N/W_W=1.5/3 (μm) will provide a stable, high-performance laterally-coupled grating.

The resonances observed in Figure 5 occur for the same reasons as in Figure 4, except now they are due to standing wave patterns in the

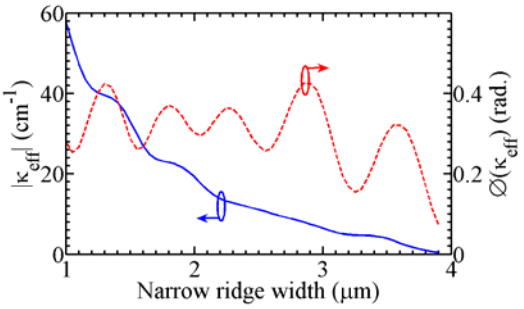

(a)

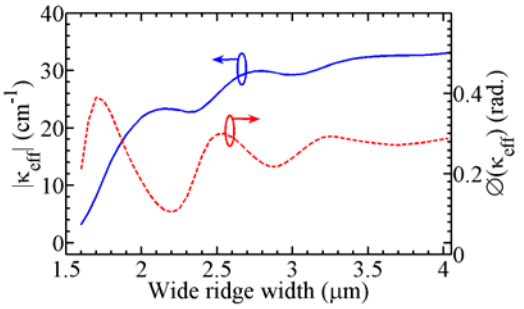

(b)

Figure 5. Effective coupling coefficient for a fourth-order grating with a duty cycle of 0.6 *vs.* a) narrow ridge width, W_N, for W_W = 4 μm, and b) wide ridge width, W_W, for W_N = 1.5 μm.

horizontal direction. Since κ_{-4} changes more steeply *vs.* grating width than *vs.* grating height, the partial wave terms, along with their resonances, have less of an impact on κ_{eff} .The result is the more subtle resonances observed in Figure 5 compared to Figure 4, where the partial wave terms predominate.

4. Conclusions

We have investigated the optical properties of fourth-order laterally-coupled gratings in terms of their effective coupling coefficient. We find that $|\kappa_{eff}|$ *vs.* duty cycle characteristic has four maxima, the two largest occurring at duty cycles of 0.58 and 0.88. There are periodic variations that occur in both the real and imaginary parts of κ_{eff} *vs.* the grating height and grating widths, W_N and W_W. Due to the predominance of the ζ_2 terms in the κ_{eff} term, the periodic variations in $|\kappa_{eff}|$ are relatively larger *vs.* the grating height than *vs.* the grating widths. In the grating ridge width characteristic, the predominance of the κ_{-4} will produce subtler resonance effects. This analysis shows that fourth-order gratings with a duty cycle with a grating height of ~0.64 μm, W_N = 1.5 μm, and W_W > 3 μm will produce a high-performance laterally-coupled grating for DFB laser applications.

5. References

1. M. Muller, F. Klopf, M. Kamp, J.P. Reithmaier, and A. Forchel, Wide range tunable laterally coupled distributed-feedback lasers based on InGaAs-GaAs quantum dots, *IEEE Photon. Technol. Lett.*, **14**, pp. 1246-1248 (2002)
2. P.K. Das, M. Uemukai, T. Suhara, InGaAs/AlGaAs Quantum Well Laterally-Coupled Distributed Feedback Laser, *Jpn. J. Appl. Phy.*, **43**, pp. 2549-2550 (2004).
3. W. Streifer, D.R. Scifres, and R.D. Burnham, Coupled wave analysis of DFB and DBR lasers, *IEEE J. Quantum Electron.,* **QE-13**, pp. 134-141 (1977)
4. W. Streifer, D.R. Scifres, and R. Burnham, Analysis of grating-coupled radiation in GaAs:GaAlAs lasers and waveguides, *IEEE J. Quantum Electron.,* **QE-12**, pp. 422-428, (1976).
5. R. Millett, K. Hinzer, T. Hall, and H. Schriemer, Fabrication-Tolerant Higher Order Laterally-Coupled Distributed Feedback Lasers, *Photonics North*, Montreal, PQ, Proc. SPIE, vol. 7099, (2008),.
6. C.H. Chen, L.H. Chen, and Q.M. Wang, Coupling coefficients of gain-coupled distributed feedback lasers with absorptive grating, *Electron. Lett.*, **32**, pp. 1288-1290, (1996).
7. R. Millett, K. Hinzer, T. Hall, and H. Schriemer, Simulation Analysis of Higher Order Laterally-Coupled Distributed Feedback Lasers, *IEEE J. Quantum Electron.*, in press, (2008).
8. Y. Zhong, X. Zhu, G. Song, Y. Huang, and L. Chen, Two-dimensional simulation of high-order laterally-coupled GaAs-AlGaAs DFB laser diodes, *Semicond. Sci. Technol.*, **19**, pp. 971-974, (2004).

9. Acknowledgements

The authors wish to acknowledge the insight and comments of Valery Tolstikhin of OneChip Photonics. This work was supported by the Ontario Centres of Excellence, Canadian Foundation for Innovation, Natural Sciences and Engineering Research Council, CMC Microsystems, OneChip Photonics, and the Ontario Graduate Scholarship Program.